CrystEngComm

Accepted Manuscript

ROYAL SOCIETY OF CHEMISTRY

www.rsc.org/crystengcomm

Effects of Mg-doping on optical and CO gas sensing properties of sensitive ZnO nanobelts

Muhammad Amin[1], Nazar Abbas Shah[*1], Arshad Saleem Bhatti[2], Mohammad Azad Malik[3]

[1] Thin Films Technology Laboratory, Department of Physics, COMSATS Institute of Information Technology, Islamabad, Pakistan; E-Mails: aminislamabad@gmail.com

[2] Centre for Micro & Nano Devices, Department of Physics, COMSATS Institute of Information Technology, Islamabad, Pakistan E-Mails: asbhatti@comsats.edu.pk

[3] School of Materials, The University of Manchester, UK, Email: azad.malik@manchester,ac.uk

Corresponding Author: nabbasqureshi@yahoo.com, Cell: +92-321-5105363

We report the synthesis, optical characterizations and enhanced carbon monoxide (CO) gas sensing properties of Magnesium (Mg) doped 1D zinc oxide (ZnO) nanobelts by vapor transport method. The structural, morphological and compositional properties of the samples were investigated by powder X-ray diffraction (p-XRD), field emission scanning electron microscopy (FESEM) and energy dispersive X-ray (EDX) analysis. Optical characterizations were carried out by Raman spectroscopy, Photoluminescence (PL), diffused reflectance spectroscopy (DRS), UV sensing and CO gas sensing. Crystalline nanobelts were obtained with the average thickness about 34 nm, width 290 nm, and length 3.25 µm. significant changes in energy bandgap was observed due to Mg doping. Undoped and Mg-doped ZnO nanostructures were tested for gas sensing properties based on resistance change under exposure to air and the CO gas. The Mg-doped ZnO nanobelts showed five times enhanced sensing properties towards 20 ppm of CO gas at 350 °C with good stability, indicating that Mg doping is very much effective in improving the CO sensing of ZnO nanobelts. In addition, a model which describes

CO gas sensing mechanism for both, undoped and Mg-doped ZnO nanostructures is also presented.

Key words: ZnO, Nanobelts, Mg doping, CO gas sensors, UV sensing

1. Introduction

1D oxide semiconductors nanocrystals are considered to be highly efficient source for gas sensing due to their high sensitivity to surface chemical reaction, rapid response and high surface to volume ratios in comparison to thin film gas sensors. Consequently, synthesis of 1D oxide semiconductors nanostructures with different morphologies and size is of significant importance from the fundamental research and the novel device development.[1-3] Among several excellent metal oxide nanomaterials, ZnO is well suited for a number of applications owing to its characteristics such as direct and wide bandgap (3.37 eV), high exciton binding energy (60 meV) at room temperature, simple fabrication and good biocompatibility.[4,5] ZnO nanostructures are therefore considered as one of the most promising gas sensing material due to its high sensitivity to toxic and combustible gases, carrier mobility, and good chemical and thermal stability at moderately high temperatures.[6] Different techniques have been applied to improve its response, reaction speed, and stability.[7,8] However, it still remains a challenge to increase the sensing response and detection limit of ID ZnO nanobelts. Many techniques such as doping,[9] fabrication of hetrostructure,[10] systematic controls of morphologies [11] and functionalization [12-14] have been used to improve the stability, sensitivity response and recovery speed of the 1D nanostructure based sensors. Doping is considered to be an effective method in for improving gas sensing properties of ZnO nanostructure at low temperature. Different researchers have used doped ZnO nanostructures for the detection of CO by using different techniques. For example Gasper *et al.*[15] showed that the doping of ZnO by transition metal ions lowers the CO detection limit by 1-2

ppm at 300°C. Mg-doped ZnO has been studied intensively due to its band gap engineering effect. One of the important features of ZnO is that by doping with Mg, increases the bandgap of ZnO.[16] Changhyun *et al*.[17] demonstrated that Mg doped ZnO nanowire sensors showed maximum response of 1.04 (4.65%) for 100 ppm of CO gas at 100 °C. Although Mg doped ZnO nanostructures have been utilized for a number of applications. To the best of our knowledge, there are reports on the synthesis of Mg doped ZnO nanostructures[18,19] but no report is available on a very thin and transparent Mg doped ZnO nanobelts using magnesium acetate in the source material *via* vapor transport method and their applications as CO gas sensors with enhanced sensing response.

In this research paper, we report the successful synthesis of very thin and transparent Mg doped ZnO nanobelts with an average thickness of 34 nm using a simple vapor transport method, vapor liquid solid (VLS) for enhanced CO gas sensing application. The effects of Mg doping on the structural, optical, morphological and gas sensing properties of ZnO nanobelts were also investigated. Toxic gases can affect human life and health even at levels of few parts per million and therefore, highly sensitive gas sensors are required. Since CO gas is tasteless, odorless and toxic and as such may not be easily detected by humans. Therefore, it is essential to develop a sensitive CO gas sensor to protect human's exposure to CO gas.

2. Experimental details

2.1. Synthesis of Mg-doped ZnO nanobelts

Vapor transport method has been used for the synthesis of undoped and Mg-doped ZnO nanostructures as shown in Fig. 1(a). Two experiments were performed under the same conditions for undoped and Mg-doped ZnO nanostructures. Ion sputtering technique was used for deposition of a thin catalyst layer (1 nm) of Gold (Au) on Si (100) substrates. Source material

containing a mixture of 99.99% pure ZnO (0.5 g) and 99.9% Graphite powder (0.5 g) for undoped and a mixture of 99.99% pure ZnO (0.5 g), 99.9% Graphite powder (0.5 g) and 0.1 g Magnesium acetate [Mg $(CH_3COO)_2 .4H_2O$] for doping of Mg was placed in ceramic boat at the centre of quartz tube (length 100 cm and diameter 3.5 cm). Substrates were placed on another ceramic boat at the downstream of the source material. This quartz tube was then mounted inside the horizontal tube furnace. The temperature of the furnace was maintained at 900 °C for 60 min in Argon (Ar) atmosphere with a constant flow rate of 50 sccm in the two experiments. The other end of quartz tube was connected with a flexible tube (diameter 1.0 cm and length 100 cm) and was kept open. Graphite powder was used to lower the evaporation temperature of ZnO (1975 °C). By introducing graphite powder in ZnO precursor, carbothermal reaction gives rise to the formation of Zn and ZnO_x (sub-oxides) vapors at 900-1000 °C as given by the reactions.[20]

$$ZnO + C \rightarrow Zn + CO \quad (1)$$

$$ZnO + CO \rightarrow Zn + CO_2 \quad (2)$$

$$ZnO + (1-x)\, C \rightarrow ZnO_x + (1-x)\, CO \ (x<1) \quad (3)$$

$$ZnO + (1-x)\, CO \rightarrow ZnO_x + (1-x)\, CO_2 \quad (4)$$

After the reaction, furnace was cooled down to room temperature. The collected nanostructure samples were characterized by FESEM equipped with EDX and X-Ray diffraction (XRD, X'Pert PRO Difractometer, PANalytical with Cu Kα radiation λ = 1.5418 Å) to find the morphologies and crystal structure. Raman spectroscopy (Renishaw, 514.5 nm laser), Photoluminescence (PL, DONGWOO Optron, 488 nm Ar laser) and EDX were used to study the Mg doping and chemical composition of ZnO nanobelts. UV-VIS diffused reflectance spectroscopy (DRS, lambda 950 UV VIS. Spectrophotometer) was utilized to find energy

bandgap of the nanostructures. CO gas sensing characterizations were carried out by measuring respective resistances by two probe method using a multimeter (Keithly 2100).

2.2. Gas sensor fabrication and characterization

The CO gas sensors were fabricated by depositing a 200 nm thick layer of SiO_2 thermally onto the single crystalline Si (100) wafers. A slurry droplet containing Mg-doped and un-doped ZnO nanobelts (20 µL) was dropped onto the SiO_2 coated Si substrates equipped with a pair of interdigitated Au (200 nm) electrodes with a gap of 50 µm through photolithography technique. These sensors were heat treated in air for 4 hours at 400°C before performing the gas sensing experiments. The sensing experiment was performed at 350°C with 5 min cycles of dry air and 20 ppm CO gas. The sensing response ($S=R_a / R_g$) of the device was measured by resistance change upon exposure to air (R_a) and CO gas (R_g) in self-designed gas chamber connected with Keithly multimeter, gas flow meters and tube furnace. The schematic design and gas sensing characterization setup have been shown in Fig. 1(b) & (c). The inset of the Fig. 1 (c) shows the sensor holder with pressure contacts. Optical fluorescent image of nanobelts sensor and microscopic image of interdigitated Au electrodes are shown in Fig. 1 (e) & (d).

3. Results and discussion

3.1. Morphology and Microstructure Analysis

The general morphology of the synthesized undoped and Mg-doped ZnO nanostructures was investigated by using FESEM, TEM and high resolution TEM. Fig. 2 (a) shows undoped ZnO nanorods with uniform diameter and length having average diameter of 168 ± 30 nm and average length of 2.4 ± 1.2 µm. Inset Fig. 2 (a) shows the magnified image of the un-doped ZnO nanorods. Fig. 2 (e) shows corresponding EDX analysis of the undoped ZnO nanorods, clearly

showing the Zn and O peaks. The approximate atomic ratios found to be 66.61: 33.39. Fig. 2 (b) shows FESEM image of Mg-doped ZnO nanobelts. Inset Fig. 2 (b) shows the magnified image of Mg-doped ZnO nanobelts. The general morphology is same *i.e.* transparent, smooth edges, uniform width along the entire length and rectangular cross section for all the nanobelts. The average thickness, width and length of the nanobelts are 34 ± 5 nm, 290 ± 160 nm and 3.25 ± 1.51μm respectively. The corresponding EDX analysis of Mg-doped ZnO sample (Fig. 2 (f)) shows the presence of oxygen, magnesium and zinc in the ratios O: Mg: Zn was found to be 30.79 (O): 3.43 (Mg): 65.78 (Zn). The aspect ratio of un-doped and Mg-doped ZnO nanostructures is found to be 14.3 and 8.5(W/T) respectively. FESEM micrographs clearly show that the morphology changes from nanorods to nanobelts due to Mg doping. The possible reason for the formation of thin and transparent nanobelts is due to the morphology transition of ZnO from nanorods to nanobelts by Mg doping because mixing/doping/alloying of specific element play a major role in modifying the dimensions of nanostructures[21, 22]. ZnO nanobelts are formed in a continuous '1D branching and subsequent 2D interspace filling' process.[23] For group II–VI semiconductors with a wurtzite crystal structure, the characteristic polar surfaces can induce asymmetric growth, leading to the formation of unique nanostructures.[24]

Fig. 2 (c) & (d) shows the high resolution TEM (HRTEM) images of undoped and Mg-doped ZnO nanostructures. The inset TEM image of Fig. 2 (c) clearly shows the catalyst particles (Au) on the tips of the nanorods suggesting the VLS growth. HRTEM image (Fig. 2 (c)) shows the lattice fringes of undoped crystalline nanostructures where as these fringes are blurred in the Mg-doped nanobelts Fig. 2 (d). The corresponding selected area electron diffraction (SAED) patterns shown in the inset of Fig. 2 (c) & (d) are consistent with the HRTEM

observations. These results confirmed the defect free growth of undoped ZnO nanorods. Similar results were reported by J. Singh et al. for the Magnesium doped ZnO nanowires.[18]

3.2. XRD and Raman spectroscopic analysis of Mg doped ZnO nanostructures

Fig. 3 (a) shows XRD patterns of undoped and Mg-doped ZnO nanostructures. All the peaks match with the hexagonal phase of ZnO (ICDD PDF-2 entry 01-079-0207). The calculated lattice parameters a = 3.2650 Å and c = 5.2278 Å are comparable to the pure ZnO a = 3.2533 Å and c = 5.2072 Å. No diffraction peaks for other impurities were observed in the XRD patterns. A slight shift in the peak position of doped samples as compared to the un-doped samples was observed as shown in the inset of Fig. 3 (a) which indicates that the Mg doping induces lattice strain in ZnO nanobelts. The lattice parameter "c" calculated from the (002) plane of the doped and the undoped samples were found to be 5.2278 Å, and 5.1840 Å respectively. The decrease (ca 0.0438 Å/ 0.83%) of this lattice parameter indicates the lattice compression along c-axis[25] caused by the replacement of Zn by Mg which has a smaller atomic radius (0.57 Å) as compared to Zn (0.60 Å).[26, 27]

Raman spectroscopic analysis at 514 nm excitation wavelength was performed to investigate the vibration properties of the undoped and Mg-doped ZnO nanostructures as presented in Fig. 3 (b). There is a significant difference between these two spectra. The peaks at 338, 436 and 579 cm^{-1} were observed for undoped ZnO nanorods. The peak at 338 cm^{-1} is attributed to the A_1 symmetry mode, the peak at 436 cm^{-1} corresponds to ZnO non-polar optical phonons E_2 (high) mode while the peak at 579 is assigned to E_1 (LO) mode which is caused due the formation of defects such as oxygen vacancies.[28] Mg-doped ZnO nanobelts showed a shift in the signals at 335 cm^{-1} and 438 cm^{-1} as compared to the pure ZnO. The peak at 438 cm^{-1} is blue

shifted with weak intensity and broadened for the Mg-doped ZnO. Usually the Raman peak shifts occurs due to three reasons: phonon confinement effects, [29] lattice strain [30] and the oxygen vacancies.[31] The broadening of the peak E_2 (high) mode can be attributed to the size effect and residual stress in the Mg doped nanobelts.[32] Therefore, in our case the blue shift in the Raman active E_1 (LO) and E_2 (high) modes of the Mg-doped ZnO nanobelts are strong evidence for successful Mg-doping in ZnO nanobelts.

3.3. Photoluminescence spectroscopy

Fig. 4 (a) & (b) shows the room temperature PL spectrum with He-Cd laser excitation at 488 nm. Both undoped and Mg-doped ZnO show broad green emission bands centered at 527 nm and 530 nm respectively. The PL results clearly show the shift in Gaussian fittings at respective bands and presence of new bands at 598 nm and 647 nm for Mg-doped ZnO nanobelts. Green emission is generally attributed to various intrinsic defects produced during synthesis of ZnO nanostructures.[33] The presence of surface defects such as oxygen vacancies (V_o), Zn vacancies (V_{Zn}), interstitial Zinc (Zn_i) and anticite defects (O_{Zn}) have been reported by different researchers corresponding to the green emission of ZnO.[34-36] In our experiment, an interesting phenomenon was observed that the intensity of the visible emission band in Mg-doped ZnO nanobelts is much stronger than the un-doped ZnO nanorods. This may be attributed to the increase in concentration of oxygen vacancies and surface recombination effects on the thin nanobelts system.[37, 38]

3.4. Diffused reflectance spectroscopy

The optical properties of undoped ZnO and Mg-doped ZnO nanobelts have been investigated by UV-visible diffuse reflectance spectroscopy. Fig. 5 (a) & (b) show the plots of $[F(R)]^2$ *vs* photon energy of synthesized nanostructures. Where F(R) is the Kubelka-Munk function which is given by the relation.[39]

$$F(R) = ((1-R)^2/2R) = (\alpha/S) \qquad (5)$$

Where *R, α*, and *S* are the diffuse reflection, absorption and scattering coefficient respectively. The bandgap can be defined by extra- ploting the linear part of the plots to the photon energy axis.[40] The optical bandgap has been calculated and found to increase from 3.18 eV for undoped ZnO nanorods to 3.32 eV for Mg-doped ZnO nanobelts, because MgO has a wider bandgap than ZnO.[41] Hsu *et al.* reported that doping with Mg increases the band gap of ZnO.[16, 42] This increase in bandgap might be due to increase in carrier concentration that blocks the lowest states in the conduction band, this effect is known as Burstein-Moss effect.[40] The schematic diagram of the energy transition mechanism from the exitonic and defects states in the undoped and the Mg-doped ZnO nanostructure is shown in Fig. 5 (c). Exitonic transition energy blue shifted to a high energy value due to Mg doping in ZnO. During the formation of the Mg: ZnO structure, Mg^{2+} ions were substituted for the Zn^{2+} ions without changing the ZnO structure. However, Mg doping in the ZnO acts as donor and the energy bandgap of the structure increases.[43] Optical properties of the synthesized ZnO nanostructures are in agreement with XRD and EDX results.

3.5 UV sensing

ZnO nanostructures are good materials for ultraviolet light sensors due to its wide bandgap (UV range for ZnO is about 368-390 nm).[44] Fig. 5 (d) shows the room temperature UV sensing results of the Mg-doped and undoped ZnO nanostructures. Sensing response of the Mg-doped ZnO nanobelts and undoped nanorods was found to be 2.32 and 1.13 respectively. Enhanced (two times) sensing response was observed for the Mg-doped ZnO nanobelts. The resistance decreases with UV light (wavelength ranges from 315 to 365 nm with 18 W UV Phillips Lamp) illumination and increases again when the UV light is switched off. When ZnO nanostructures sensor is exposed to air, the negative space charge layer on the surface is created and the adsorbed oxygen molecule captures an electron from the conduction band (sensor exhibits higher resistivity). When the energy of photon is greater than the energy bandgap E_g, radiation is absorbed by the nanostructures sensor, creating an electron-hole pair. The photo-generated, positively-charged hole neutralizes the chemisorbed oxygen responsible for the higher resistance, increasing the conductivity of the device. As a consequence, the conductivity in the material increases giving rise to photocurrent. This process goes on in a cyclic manner with the on-off switching of the UV light. The enhanced response in the case of Mg-doped ZnO belts was attributed to the energy levels introduced by the dopant in the corresponding bandgap and in the conduction band of ZnO. These states acted as the "hoping" states and increase the excitation probability of an electron to the conduction band.[45]

3.6 Characterization of CO gas sensors

Fig. 6(a) & (b) show the sensing response signals of the doped and undoped ZnO nanostructures. Previous reports showed that response of resistive sensors is highly affected by the operating

temperature. Therefore, in order to optimize the operating temperature of Mg-doped ZnO nanobelts, sensors were tested at different temperatures ranging from 200 °C to 400 °C for 20 ppm of CO gas as shown in Fig. 6 (d). It was observed that sensing response increases with increase in working temperature and reached a maximum at about 350 °C and then started decreasing. At low temperature CO molecule are not activated enough to react with the surface adsorbed oxygen species. Above 350 °C, the decrease in CO gas adsorption is not adequately compensated by the increase of surface reaction and the sensor response decreases. This behavior may be interpreted on the basis of adsorption/desorption and reaction processes taking place on the surface of sensing layer.[46] The sensing experiment was performed at 350 °C with 5 min cycles of dry air and 20 ppm CO gas. The resistance decreased upon exposure to CO and recovered completely to the initial value upon removal of CO. Sensing response of the undoped nanorods and Mg-doped ZnO nanobelts was found to be 1.05 and 5.5 respectively. Enhanced (five times) sensing response was observed for the Mg-doped ZnO nanobelts. Response and recovery times of both sensors were nearly equal as shown in Fig. 6 (a) & (b). Mg-doped ZnO nanobelts are capable to adsorb large amount of oxygen due to larger surface area (greater number of defects) which increases the chance of ZnO interacting with CO gas and fast chemisorptions/desorption properties of the CO gas at 350 ºC as compare to undoped ZnO nanostructures.[47,48] N. Hongsith et al. reported that the sensor response is proportional to the reaction rate constant k_{co} (T) and k_{oxy} (T), through oxygen density which is given by the following equation.[49]

$$S = R_a/R_g = (\square_t\, k_{co}\,(T)\, k_{oxy}\,(T)\, [O^{ion}_{ads}]^{\,b}\, [CO]^{\,b})/n_0 + 1. \qquad (6)$$

Where R_a = resistance in air, R_g = resistance in gas, τ_t = Time constant, $[O^{ion}_{ads}]^b$ = Chemisorbed Oxygen concentration, $[CO]^b$ = CO concentration, b = charge parameter and n_0 = carrier concentration in air.

3.7 Sensing mechanism: Band theory model

In order to explain the sensing mechanism (shown in Fig. 6 (c)), the band theory was applied to gas sensors which have been the subject of intense study for a number of years.[50, 51] The sensing mechanism is based on the principal of change in electrical resistivity /conductivity as a result of chemical reaction between gas molecules and the reactive oxygen ions on the surface of ZnO nanostructures. The change in electrical conductance is given by equation (2).[52]

$$\Delta G = \frac{1}{R} = \frac{\left(\Delta n_o |e| \mu \pi r^2\right)}{l} \qquad (7)$$

Where l is length of the nanostructure channel, r is the radius, μ is electron mobility e is electron charge and Δn_o represents the change in carrier concentration. When the surface of the undoped and Mg-doped ZnO nanostructures is exposed to the air, the oxygen which takes part in detection procedure is consequently ionized into dynamic oxygen species (O^{2-}, O_2^- and O^-) while moving from site to site by capturing electrons from active surface sites of un-doped and Mg-doped ZnO nanobelts.[53, 54] At high temperature reactive oxygen species are chemisorbed by these ZnO nanostructures as a result electron transfer takes place. When the adsorption reaches a certain level, a thick depletion layer is formed due to which decrease in carrier concentration takes place and this result in increased resistance of the material. In contrast, when undoped and Mg-doped ZnO is exposed to the CO gas chemical reaction takes place as adsorbed oxygen ions produce

CO_2 which leads to increase in carries concentration and a decrease in resistance.[55] the mechanism can be summarized by the following chemical reactions.

$$O_{2\,(gas)} \rightarrow O_{2\,(ad)} \quad (8)$$

$$O_{2\,(ad)} + e \rightarrow O_{2\,(ad)}^{-} \quad (9)$$

$$O_{2\,(ad)}^{-} + e \rightarrow 2O_{(ad)}^{-} \quad (10)$$

$$2CO + O_{2\,(ad)}^{-} + e \rightarrow 2CO_{2\,(gas)} + e^{-} \quad (11)$$

$$CO + 2O^{-} \rightarrow CO_3^{2-} \rightarrow CO_2 + 1/2O_2 + 2e \quad (12)$$

Table 1 shows the summary of the results which are systematic. Morphology of the synthesized ZnO Nanostructures changes by Magnesium doping. PL and Raman peak positions are found to be shifted and new peaks were observed which confirms Mg doping in ZnO, Band gap of ZnO nanostructures increases due to defects states as a result of Mg-doping and hence the CO gas sensing response increases about five times as compared to the undoped ZnO nanostructures.

Conclusion

Magnesium doped ZnO nanobelts were successfully synthesized using magnesium acetate as source material by vapor transport method. A clear change was observed in the morphology from ZnO (nano rods) to Mg-doped ZnO (nano belts). Shifts in the XRD peaks in Mg-doped samples as compared to ZnO were an indication that Mg has substituted Zn in the ZnO lattice. The doping was also confirmed by EDX, photoluminescence and Raman spectroscopy. The gas sensor fabricated from multiple networks of the Mg-doped ZnO nanobelts showed enhanced signal responses to 20 ppm of CO gas at 350 °C. The gas sensing response of the Mg-doped ZnO nanobelts sensor was improved five times in comparison to undoped ZnO nanorods sensor. The

enhanced signal response was attributed to the catalytic effect of dopant, defects, like oxygen vacancies (potential barrier modification) and fast chemisorptions and desorption properties of the CO gas. Band theory model was adopted to explain the possible sensing mechanism of the Mg-doped ZnO nanostructures.

Acknowledgements

The authors would like to thank Higher Education Commission (HEC) of Pakistan for the financial support through ‘‘National Research Program for Universities” and for the award of Indigenous 5000 PhD scholarship program batch-IV. We would also like to thank COMSATS Institute of Information Technology, Islamabad for providing excellent research facilities and Institute of Industrial Control Systems. The authors are grateful to Dr Ahmer Naveed (Centre for Micro & Nano Devices, Department of Physics, COMSATS Institute of Information Technology, Islamabad, Pakistan) and Rizwan-ur-Rehman Sagar (School of Materials Science and Engineering, Tsinghua University, Haidian Beijing, China) for useful discussions.

References

1 C. Liuangyanb, L. Zhiyonga, B. Shoulia, Z. Keweia, L. Dianqinga, C. Aifana, L.C. Chiun, Sens. Actuat. B, 2010, 143, 620-628.

2 A. Kolmakov, Y. Zhang, G. Cheng, M. Moskovits, Adv. Mater. 2003, 15, 997-1000.

3 Y. Liu, E. Koep, M. Liu, Chem. Mater. 2005, 17, 3997-4000.

4 X.J. Huang, Y.K. Choi, Sens. Actuat. B, 2007,122, 659-671.

5 Y. Qiu, S. Yang, Adv. Fun. Mat, 2007, 17, 1345-1352.

6 T. Gao, T.H. Wang, Appl. Phys. A, 2005, 80, 1451-1454.

7 R.C. Wang, H.Y. Lin, Sens. Actuat. B, 2010, 149, 94-97.

8 V. Kobrinsky, E. Fradkin, V. Lumelsky, A. Rothschild, Y. Komem, Y. Lifshitz, Sens. Actuat. B, 2010, 148, 379-387.

9 Q. Wan, T. H. Wang, Chem. Commun., 2005, 3841-3843.

10 X. Xue, L. Xing, Y. Chen,; S. Shi, Y. Wang, T. Wang, J. Phys. Chem. C, 2008, 112, 12157-12160.

11 M. Amin, U. Manzoor, M. Islam, A.S. Bhatti, N.A. Shah, Sensors, 2012, 10, 13842-13851.

12 A. Kolmakov, D. O. Klenov, Y. Lilach, S. Stemmer, M. Moskovits, Nano Lett., 2005, 5, 667-673.

13 Q. Kuang, C. S. Lao, Z. Li, Y. Z. Liu, Z. X. Xie, L. S. Zheng, Z. L. Wang, J. Phys. Chem. C, 2008, 112, 11539-11544.

14 A. Wei, L. Pan, W. Huang, Mat. Sci. Eng. B, 2011, 176, 1409-1421.

15 E.D. Gaspera, M. Guglielmi, G. Perotto, S. Agnoli, G. Granozzi, M.L. Post, A. Martucci, Sens. Actuat. B, 2012, 161, 675-683.

16 H.C. Hsu, C.Y. Wu, H.M. Cheng, Z.Y. Wang, J.W. Zhao, L.D. Zhang, Appl. Phys. Lett., 2006, 89, 013101-013103.

17 C. Jin, S. Park, H. Kim, S. An, C. Lee, Bull. Korean Chem. Soc., 2012, 33, 1993-1997.

18 J. Singh, P. Kumar, K. S. Hui, K. N. Hui, K. Ramam, R. S. Tiwaria, O. N. Srivastava, CrystEngComm, 2012, 14, 5898-5904.

19 L. Hang, Z. Hui-zhao, X. Cheng-shan, W. Jie, L. Jun-lin, Semiconductor Photonics and Technology 2009, 15, 225-229.

20 N. Wang, Y. Cai, R.Q. Zhang, Materials Science and Engineering, 2008, 60, 1-51.

21 M. Hafeez, U. Manzoor, A. S. Bhatti, B. Karnayar and S. I. Shah, J. Appl. Phys., 2012, 111, 024313-024320.

22 H. J. Fan, B. Fuhrmann, R. Scholz, C. Himcinschi, A. Berger, H. Leipner, Nanotech., 2006, 17, 231-239.

23 J.H. Park, H.J. Choi, Y.J. Choi, S.H. Sohn, J.G. Park, Mater. Chem., 2004, 14, 35-36.

24 Z.L. Wang, X.Y. Kong, J.M. Zuo Phys. Rev. Lett. 2003, 91, 185502.

25 F. Wang, C. Zhao, B. Liu, S. Yuan, J. Phys. D: Appl. Phys., 2009, 42, 115411-115414.

26 H. Ryoken, N. Ohasahi, I. Sakaguchi, Y. Adachi, S. Hishita, H. Haneda, J. Cryst. Growth, 2006, 287, 134-138.

27 U. Ozgur, Y.I. Alivov, C. Liu, A. Teke, M.A. Reshchikov, S. Doan, V. Avrutin, S.J. Cho, H. Morkoc, J. Appl. Phys., 2005, 98, 041301-041403.

28 A. Umar, S.H. Kim, Y.S. Lee, K.S. Nahm, Y.B. Hahn, J. Cryst. Growth, 2005, 282, 131-136.

29 K.F. Lin, H.M. Cheng, H.C. Hsu, W.F. Hsieh, Appl. Phys. Lett., 2006, 88, 263117-263120.

30 A. Tiwari, M. Park, C. Jin, H. Wang, D. Kumar, J. Narayan, J. Matter. Res., 2002, 17, 2480-2487.

31 P. Jiang, J.J. Zhou, H.F. Fang, C.Y. Wang, Z.L. Wang, S.S. Xie, Adv. Funct. Mat., 2007, 17, 1303-1310.

32 C. Geng, Y. Jiang, Y. Yao, X. Meng, J. A. Zapien, C. S. Lee, Y. Lifshitz, S. T. Lee, Adv. Funct. Mater, 2004, 14, 589-594.

33 Y. Zhang, X. Song, J. Zheng, H. Liu, X. Li, L. You, Nanotech. 2006, 17 1916-1921.

34 K. Vanheusden, C.H. Seager, W.L. Warren, D.R. Tallant, J.A. Voigt, Appl. Phys. Lett., 1996, 68, 403-405.

35 Y.W. Heo, D.P. Norton, S.J. Pearton, J. Appl. Phys., 2005, 98, 073502-073505.

36 B. Lin, Z. Fu, Y. Jia, Appl. Phys. Lett., 2001, 79, 943-946.

37 I. Shalish, H. Temkin, V. Narayanamurti, Phys. Rev. B,2004, 69, 245401-245404.

38 S.A. Studenikin, M. Cocivera, J. Appl. Phys., 2002, 91, 5060-5065.

39 M. Nagasawa, S. Shionoya, J. Phys. Soc. Jpn., 1971, 30, 158-167.

40 E. Burstein, Phys. Rev., 1954, 93, 632-633.

41 D. Qiu, H. Wu, N. Chen, Phys. Lett., 2003, 20, 582-584.

42 K. S. Ahn, Y. Yan, S. Shet, T. Deutsch, J. Turner; M. Al-Jassim, Appl. Phy. Lett., 2007, 91, 231909-231912.

43 S.C. Saime, U. Ibrahim, S.S. Arda Aytimur Suleyman Ozcelik, Ceram. Int., 2012, 38, 420-4208.

44 S. Hullavarad, N. Hullavarad, D. Look, B. Claflin, Nanoscale Res. Lett., 2009, 4, 1421-1427.

45 C.S. Lao, M.C. Park, Q. Kuang, Y.L. Deng, A.K. Sood, D.L. Polla, and Z.L. Wang, J. Am. Chem. Soc., 2007, 129, 12096-12097.

46 T. Krishnakumara, R. Jayaprakashb, N. Pinnac,f, N. Donatod, A. Bonavitae, G. Micalie, G. Neri, Sensors and Actuators B 2009, 143, 198-204.

47 Y. Zhang, J.Q. Xu, Q. Xiang, H. Li, Q.Y. Pan, P.C. Xu, J. Phys. Chem. C 2009, 113, 3430-3435.

48 A.A. Ibrahim, G.N. Dar, S.A. Zaidi, A. Umar, M. Abaker, H. Bouzid, S. Baskoutas, Talanta, 2012, 93, 257-263.

49 N. Hongsith, E. Wongrat, T. Kerdcharoen, S. Choopun, Sens. Actuat. B 2010,144, 67-72.

50 F. George, L.M. Fine, A.A. Cavanagh, B. Russell, Sensors, 2010, 10 5469-5502.

51 S.R. Morrison, Sens. Actuat. B., 1981, 2, 329-341.

52 S. Osswald, M. Havel, G. Yury, J. Raman Spectrosc., 2007, 38, 728-736.

53 G.N. Ara, A. Umarb, S.A. Zaidib, A.A. Ibrahimd, M. Abakera, S. Baskoutasc, M.S. Al-Assiri, Sens. Actuat. B, 2012, 173, 72-78.

54 N. Han, L. Chai, Q. Wang, Y. Tian, P. Deng, Y. Chen, Sens. Actuat. B, 2010, 147, 525-530.

55 J. Li, H.Q. Fan, X.H. Jia, J. Phys. Chem. C, 2010, 114, 14684-14691.

Figure Captions

Figure 1 Schematic diagram of experimental setup (a) synthesis of ZnO nanostructure (b) CO gas sensing setup (c) Actual image of gas sensing setup. Inset shows sensor with holder (d) Optical fluorescent image of nanobelts sensor (e) Microscopic image of interdigitated Au electrodes

Figure 2 (a) FESEM images of undoped ZnO nanorods inset shows magnified image (b) FESEM image of Mg-doped transparent ZnO nanobelts inset shows magnified image (c) and (d) shows HRTEM images of undoped nanorods and Mg-doped nanobelts, Inset of (c) and (d) shows the magnified TEM images with corresponding SEAD images (e) and (f) shows EDX analysis of the undoped ZnO nanorods and Mg-doped ZnO nanobelts.

Figure 3 (a) X-ray diffraction analysis of un-doped and Mg-doped ZnO nanostructures. The inset figure clearly shows a slight shift in the peak position of doped samples. (b) Raman spectra of undoped ZnO nanorods and Mg-doped ZnO nanobelts.

Figure 4 Room temperature PL spectra of (a) undoped ZnO nanorods deconvoluted into three Gaussian peaks (b) Mg-doped ZnO nanobelts fitted with four Gaussian peaks.

Figure 5 plots of $F^2(R)$ vs. Energy (eV) of (a) undoped ZnO nanorods and (b) Mg-doped ZnO nanobelts. The inset figure shows the respective reflectance spectra. (c) Schematic representation

of the energy transition mechanism in the undoped and the Mg-doped ZnO nanostructures. (d) UV sensing response of Mg-doped ZnO nanobelts and undoped ZnO nanorods

Figure 6 Signal response and recovery profile of (a) undoped ZnO nanorods (b) Mg-doped ZnO nanobelts (c) Schematic of possible mechanism of how Mg-doped ZnO nanobelts sensor responses to CO in air and gas (d) Response temperature curve shows response increases till 350°C then decreases.

Table 1: Summary of the results

Morphology of nanostructures	**Synthesis Temp. (°C)**	**Band gap by UV-VIS (eV)**	**Nanostructure size**	**Aspect ratio**	**20 ppm of CO gas Response at 350°C**	**PL peak positions (nm)**	**Raman peak positions (cm^{-1})**
Nanorods (undoped)	900	3.20	D_{av}= 168 nm L_{av} = 2.4 µm	14.3	1.05	527.4 558.1	338.8 435.5 576.5
Nanobelts (Mg-doped)	900	3.33	T_{av} = 34 nm L_{av} = 3.25 µm W_{av}= 290 nm	8.5(W/T)	5.41	530.2 567.2 598.2 647.7	335.6 437.7 553.2

Figure 1

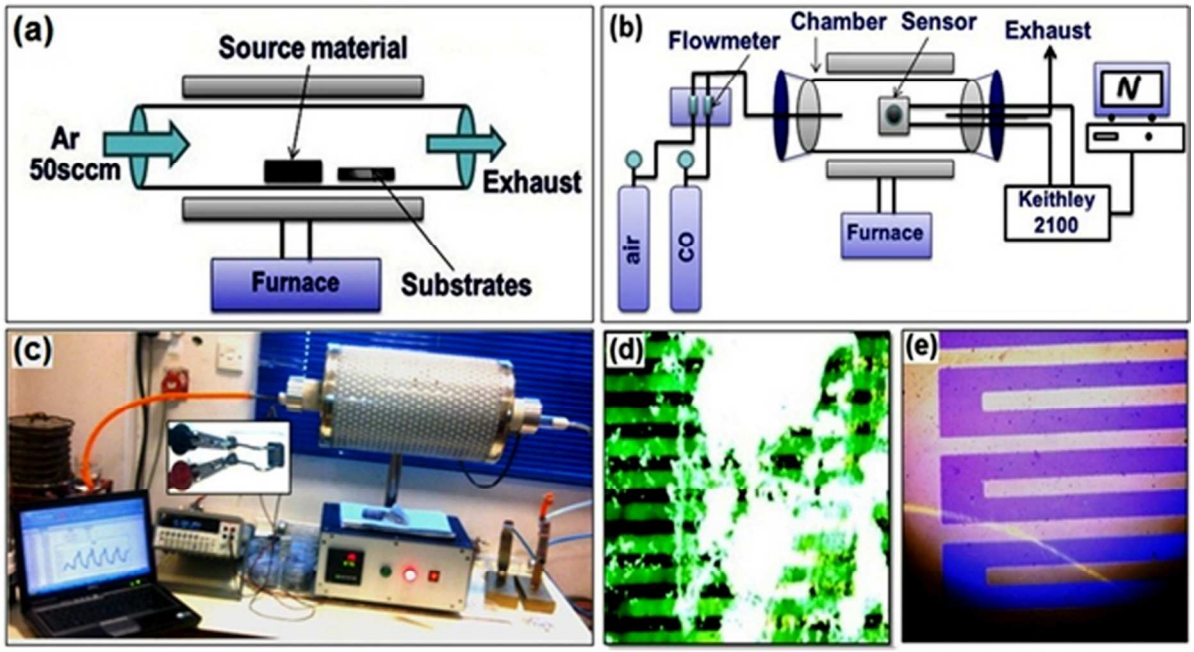

Figure 2

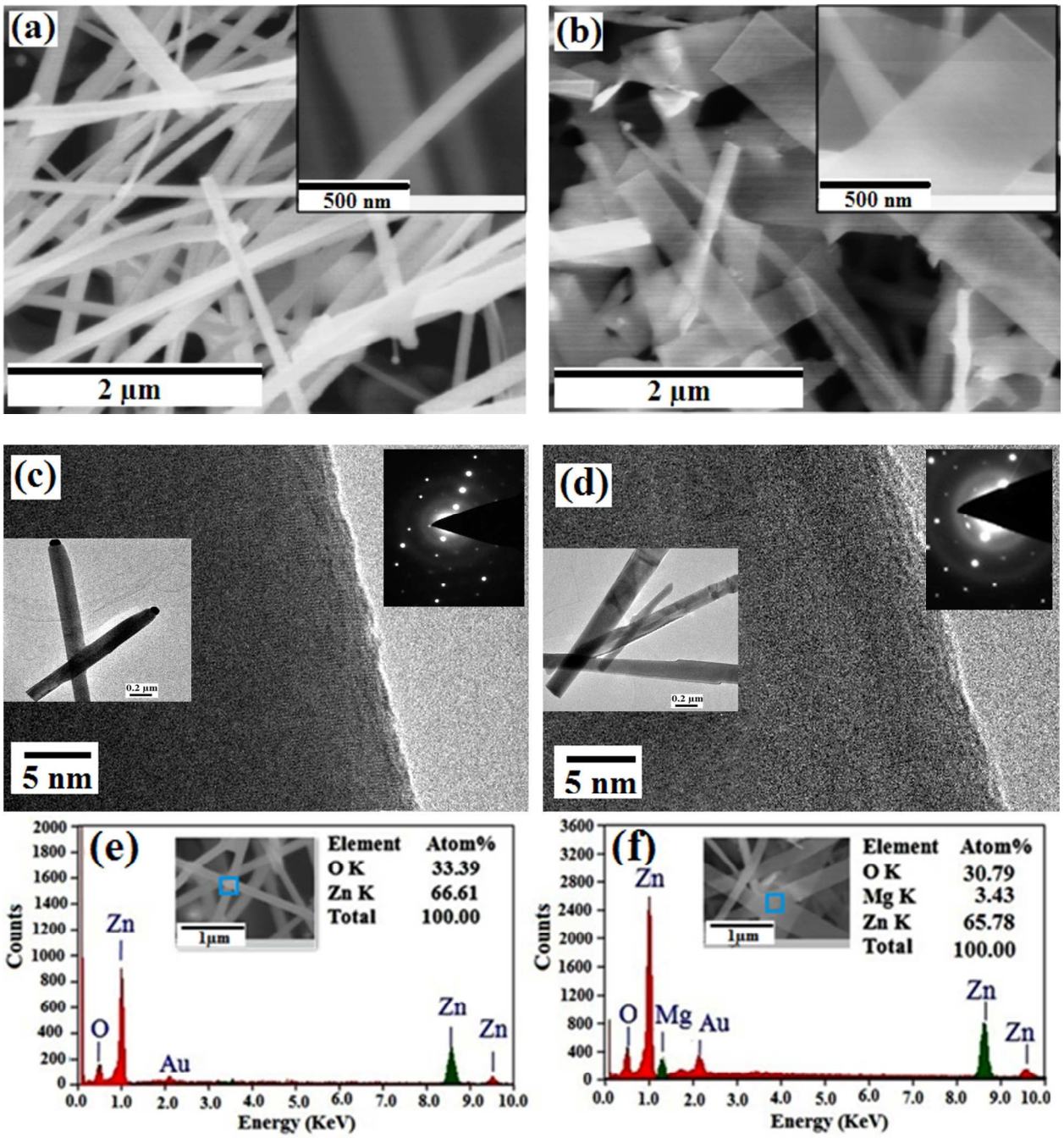

Figure 3

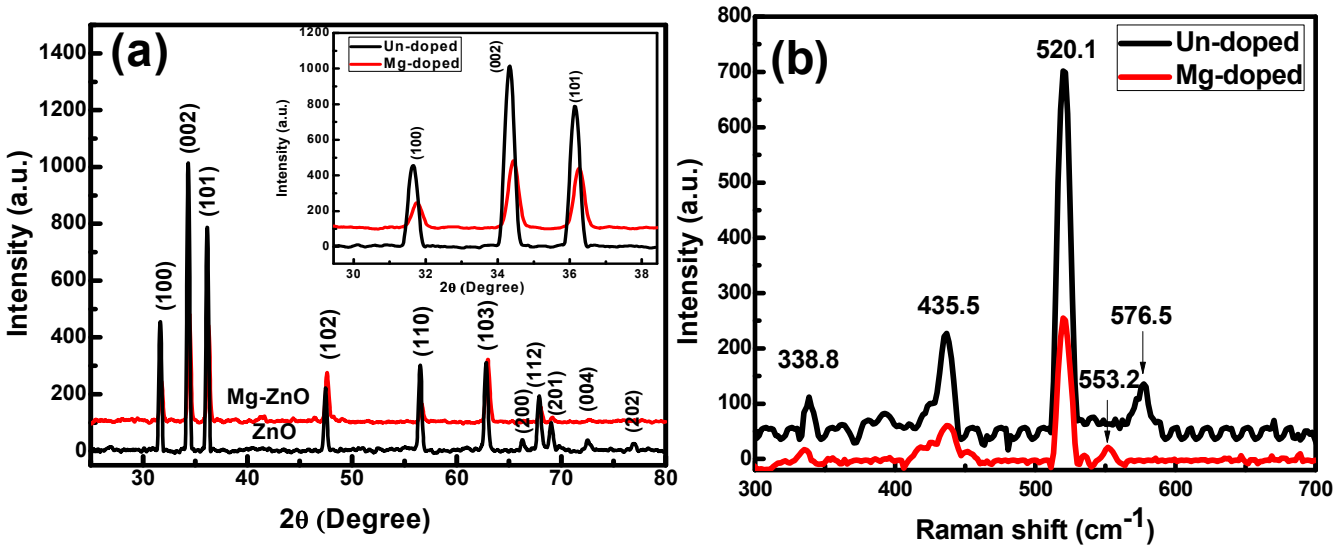

Figure 4

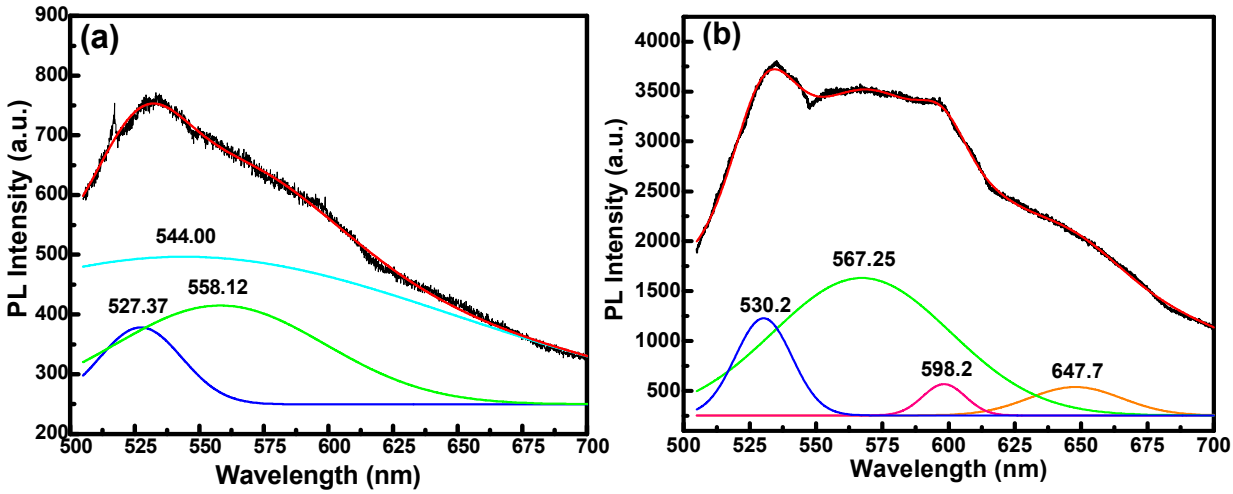

Figure 5

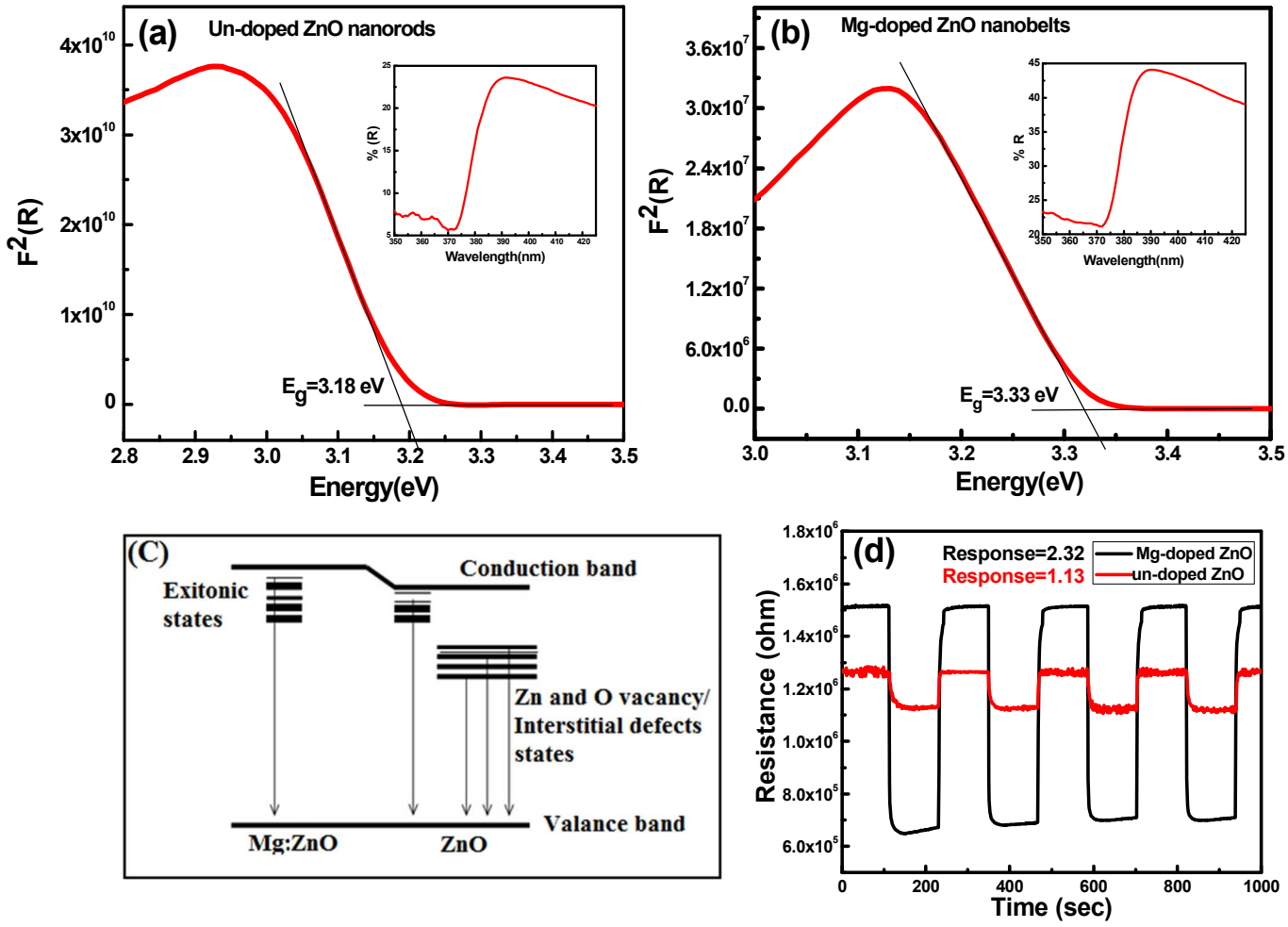

Figure 6